



Sea state contributions to thermosteric sea-level in high-resolution ocean-wave coupled simulations

Antonio Bonaduce^{1,2,3} · Nam Thanh Pham¹ · Joanna Staneva¹ · Sebastian Grayek¹ · Roshin P. Raj^{2,3} · Øyvind Breivik^{4,5}

Received: 22 March 2024 / Accepted: 24 July 2024 / Published online: 20 August 2024
© The Author(s) 2024

Abstract

This study examines the impact of wave-induced processes (WIPs) in modulating thermosteric sea-level changes, highlighting the need to include these processes in future sea-level rise assessments and climate projections. The impact of wave-induced processes on thermosteric sea-level changes is investigated using coupled ocean-wave simulations. These simulations include the effects of Stokes-Coriolis forcing, sea-state dependent surface stress and energy fluxes, and wave-induced mixing. The experiments use a high-resolution configuration of the Geesthacht COAstal Model SysTem (GCOAST), covering the Northeast Atlantic, the North Sea and the Baltic Sea. The GCOAST system uses the Nucleus for European Modelling of the Ocean (NEMO) ocean model to account for wave-ocean interactions and ocean circulation. It is fully coupled with the WAM spectral wind wave model. The aim is to accurately quantify the sea state contribution to thermosteric sea level variability and trends over a 26-year period (1992–2017). The ability of wave-ocean coupled simulations to reveal the contribution of sea state to sea level variability and surge is demonstrated. It is clear that wave-induced processes (WIPs) play a significant role in sea surface dynamics, ocean mixing (mixed layer thickness) and modulation of air-sea fluxes (e.g. heat flux) in both winter (10–20%) and summer (10%), which in turn affect thermosteric sea level variability. The North Atlantic (in summer) and the Norwegian Trench (in winter) show significant contributions (40%) to the thermosteric sea-level variability due to wave-induced processes. The influence of WIPs on thermosteric sea level trends in the North Atlantic is up to the order of 1 mm yr⁻¹ in both winter and summer, in the open ocean and at the shelf break. Smaller contributions are observed over the shelf areas of the North Sea. This study underscores the crucial role of WIPs in modulating sea-level changes and highlights the importance of including these processes in future sea-level rise assessments and climate projections.

Keywords Sea-state · Ocean-wave interactions · Thermosteric sea-level · Trend

1 Introduction

Sea level change and its impact on coastal zones have been attracting widespread interest from the natural, social scientific communities, practitioners, and policymakers

(Oppenheimer et al. 2019). The global sea level change is primarily caused by the thermal expansion of ocean water, the thawing of ice and glaciers, and the redistribution of the water cycle (Church et al. 2013; Frederikse et al. 2020). At the regional scale, sea level change depends on the transport of heat, salt, and terrestrial water storage (Stammer et al. 2013; Storto et al. 2019). The consequences of sea level rise, such as coastal erosion, flooding, and saltwater intrusion, are expected to increase significantly in the future, posing a threat to human communities in low-lying coasts and islands (Wahl et al. 2018). Over the past decade, numerous studies have examined sea-level changes at both global (Cazenave and Remy 2011) and regional scales (e.g. Bonaduce et al. 2016), analyzing the signals among various components of variability (Dangendorf et al. 2019; Frederikse et al. 2020). Hu and Bates (2018) compared steric sea-level and air temperature from climate predictions and found that sea-level

Responsible Editor: Jia Wang

✉ Antonio Bonaduce
antonio.bonaduce@nersc.no

- ¹ Helmholtz-Zentrum Hereon, Geesthacht, Germany
- ² Present Address: Nansen Environmental and Remote Sensing Center, Bergen, Norway
- ³ Bjerknes Center for Climate Research, Bergen, Norway
- ⁴ Norwegian Meteorological Institute, Bergen, Norway
- ⁵ University of Bergen, Bergen, Norway

rise during the twenty-first century is expected to be greater than during the twentieth century, even if greenhouse gas emissions were to stop now. This is due to the larger thermal inertia of the ocean compared to the atmosphere. Therefore, it is crucial to enhance our comprehension of the processes that influence the expression of steric sea-level change at different temporal and spatial scales of variability. Steric sea-level variability is driven by both temperature (thermohaline) and salinity (halohaline) variations, which modify the density structure of the water column and, in turn, change the height of the water column (Mellor and Ezer 1995; Storto et al. 2019).

Thermohaline sea-level rise was a major contributor to 20th-century sea-level rise and is projected to continue during the twenty-first century and for centuries into the future (Bindoff et al. 2007; Meehl et al. 2007). The in-depth characterization of the processes affecting the sea-level variability due to ocean thermal expansion and freshwater content is a fundamental step to describe the steric sea-level variability during the last decades (Chaigneau et al. 2022) and estimate reliable trends as a reference to assess the sea-level changes and rise milestones (Fox-Kemper et al. 2023) shown by the projections under the different climate scenarios. Ocean subsurface changes are influenced by atmospheric and oceanic conditions through wind-induced vertical mixing, heat exchange, and upwelling (Hurrell and Deser 2009). Ocean wind-generated waves (i.e., surface gravity waves) are an important component of the Earth's climate system. They have been proven to modulate the interaction between the ocean and the atmosphere in terms of mass, heat, and momentum (Hemer et al. 2013; Bonaduce et al. 2019; Breivik et al. 2019).

Ocean waves affect ocean circulation through various processes, including turbulence caused by breaking waves, momentum transfer from breaking waves to currents in deep and shallow water, wave interaction with planetary and local vorticity, Stokes drift, and Langmuir turbulence (Breivik et al. 2015; Alari et al. 2016). Wave-induced processes (WIPs) have direct effects on ocean circulation, which can be observed from the ocean surface to the mixed layer depth (MLD) (Hu and Wang 2010; Chen et al. 2021), and even deeper indirectly (Breivik et al. 2015). Staneva et al. (2017) have shown that WIPs are responsible for these effects. Recent studies have highlighted the importance of wave-induced processes in contributing to sea-level variability and trends along global coastlines. It is suggested that these processes may have been previously underestimated (Melet et al. 2018; Dodet et al. 2019), emphasizing the need to consider the changing nonlinear interactions between sea-level components caused by sea-level rise (Arns et al. 2017). Bonaduce et al. (2020) demonstrated the ability of ocean-wave simulations to reveal the impact of sea-state on sea-level variability in European Seas. The authors argued

that wind-induced pressure anomalies significantly influence surges in both open ocean and shelf areas. They recommended further investigations to assess sea-state contributions to sea-level variability and trends over a multidecadal temporal scale. Based on those results and recommendations, this study is a follow-up to Bonaduce et al.'s (2020) research. Similar methods were used to evaluate the impact of sea-state on thermohaline sea-level variability and trends from 1992 to 2017. It aims to assess the impact of WIPs on heat and mass exchanges between the ocean and atmosphere, as well as the vertical distribution of ocean temperature, and how these factors affect thermohaline sea-level. This has not been investigated in detail before.

The paper is structured as follows: after this introduction, Sect. 2 describes the ocean-wave coupled modelling system used in this study, the experimental set-up designed to investigate sea-state contributions to thermohaline sea-level variability, and the observation datasets used to assess the skill of the OGCM simulations. The synergy with observational records and the effect of WIPs on temporal evolution of temperature and salinity profiles over the GCOAST domain is presented in Sect. 3. The sea-state contribution to thermohaline and halohaline sea-level variability and trend are discussed in Sect. 4 and Sect. 5, respectively. Section 6 summarizes and concludes.

2 Methodology

2.1 Models

GCOAST is a modeling framework that integrates atmospheric, oceanic, wave, bio-geochemical, and hydrological components to address the complex interactions within the Earth's system (Staneva et al. 2018). To investigate the effect of wave-induced processes on thermohaline sea level, an ocean-wave coupled system was utilized, with its spatial domain illustrated in Fig. 1.

The ocean circulation is represented using the Nucleus for European Modelling of the Ocean (NEMO) OGCM (NEMO v3.6; Madec et al. 2019). The NEMO configuration used within the GCOAST system covers the Baltic Sea, the Danish Straits, the North Sea and has a large extent in the North Atlantic at an eddy-resolving spatial resolution of ~3.5 km. The water column is discretized using 50 hybrid s - z^* vertical levels with partial cells to fit the bottom depth shape. The NEMO set-up employed in this study is based on the one used by Bonaduce et al. (2020) to investigate sea-state contributions to surge, with the exception of a much longer temporal integration period, spanning from 1992 to 2017, and different initial conditions. The lateral open boundary and initial condition fields, including temperature, salinity, velocities, and sea level, are obtained from the Mercator

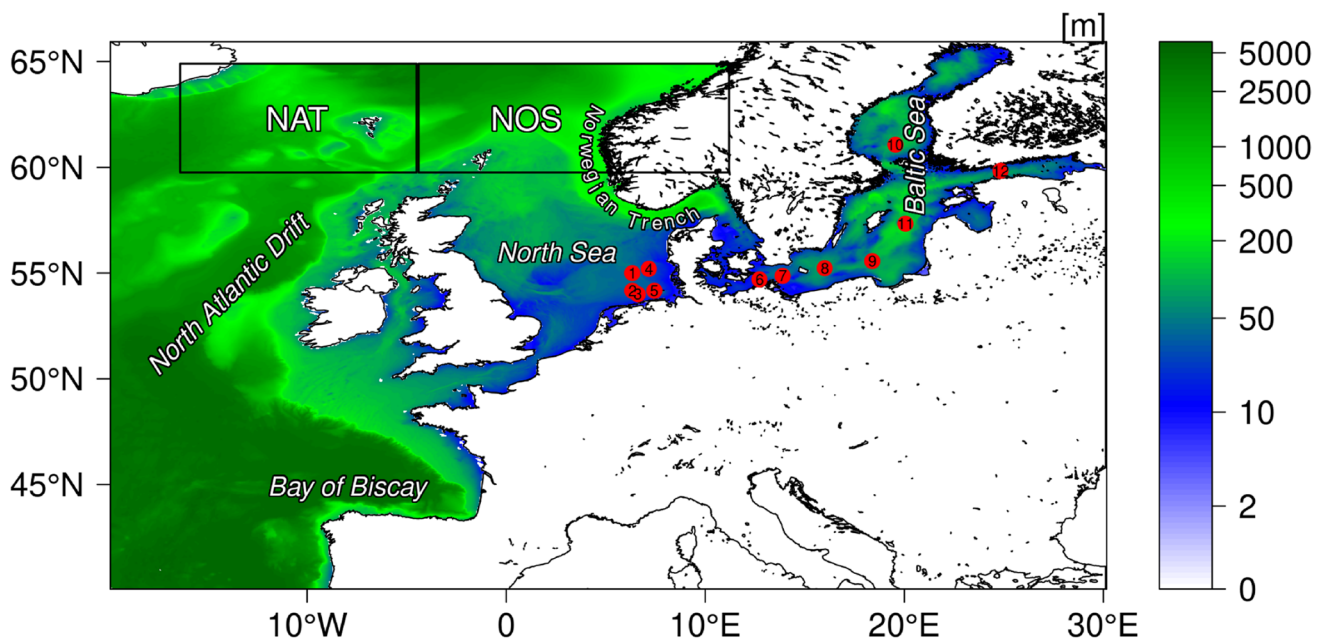


Fig. 1 GCOAST system spatial domain and two investigated sub-regions: NAT and NOS. The red dots show the geographical positions of the in-situ observations used to assess the numerical experiments: 1) NsbII (1992–2017); 2) Ems (1992–2017); 3) FINO-1 (2003–2017); 4) FINO-3 (2014–2018); 4) DeutscheBucht; 6) Darsser (1995–2017); 7) Arkona (2002–2017); 8) Helcom-097, 9) Helcom-127, 10) Helcom-157, 11) Helcom-164, 12) Helcom-275 (1992–2017). Background: GCOAST bathymetry; values are expressed as meters (m)

Ocean International Global Ocean Reanalysis (GLORYS12, Gasparin et al. 2018; Lellouche et al. 2018) and the Met Office Forecasting Ocean Assimilation Model (FOAM) AMM7 (O’Dea et al. 2012; Lewis et al. 2019) outputs. The data is currently available through the Copernicus Marine Environment and Monitoring Service (CMEMS).

Ocean-wave simulations were conducted using the WAM spectral wave model. This model represents the physics of the wave evolution for the full set of degrees of freedom in a 2D wave spectrum. A full description can be found in WAMDI-Group (1988), Komen et al. (1994), Günther et al. (1992), Janssen (2004), and ECMWF (2019). In this application, the WAM (Cycle 4.7) model runs in shallow water mode, including bottom-induced wave breaking on a model grid located between 40° N to 65° N and -19° W to 30° E, with a spatial distribution of $\Delta\phi \times \Delta\lambda = 0.03^\circ \times 0.05^\circ$ (~3.5 km). The 2D wave spectra are calculated for 24 directional bands at 15° each, starting at 7.5°, and measured clockwise with respect to true north, and 30 frequencies are logarithmically spaced from 0.042 to 0.66 Hz at intervals of $\Delta f/f = 0.1$. The underlying bathymetry is based on the one-minute global General Bathymetric Chart of the Oceans (GEBCO; <http://www.gebco.net>) topography. Regional wave model results are stored hourly, driven by ERA5 wind fields at 10 m above the surface (U10; 1-hourly; spatial resolution of 0.25°) produced by a dedicated version of the coupled ocean-wave-atmospheric model system (IFS

Cycle 41r2 4D-Var) of the ECMWF European Centre for Medium-Range Weather Forecasts (ECMWF). The NEMO ocean model has been modified to account for the following wave effects computed by WAM, as described by Staneva et al. (2017) and Alari et al. (2016): Stokes-Coriolis forcing (Wu et al. 2019), sea state dependent momentum and energy fluxes, and wave-induced mixing. A description of the wave-induced forcing and its interaction with the ocean circulation is given in Appendix 2 following Bonaduce et al. (2020). The NEMO and WAM models are coupled using the OASIS Model Coupling Toolkit (OASIS3-MCT; Valcke 2013; Craig et al. 2017), which allows numerical simulations to exchange synchronised information representing different components of the Earth system (Sterl et al. 2012; Wahle et al. 2017; Varlas et al. 2018). In wave-coupled simulations, surface stress, Stokes drift, significant wave height, mean wave period and wave-induced turbulent energy flux fields are passed from the wave model WAM to the hydrodynamic model NEMO. WAM receives sea surface height and ice concentration from NEMO.

2.2 In-situ and remote-sensing observations

Figure 1 shows how numerical simulations were compared to in-situ observations across various domains. The German Federal Maritime and Hydrographic Agency (BSH) operates the MARNET monitoring network, which includes several

monitoring stations in the German Bight and the western Baltic Sea. Ocean temperature and salinity profiles were obtained from this network. These stations automatically record marine data, such as temperature, salinity, and currents, with a temporal resolution of one hour or less. The data used in this study were obtained from the Copernicus Marine Environment and Monitoring Service (CMEMS) and the International Council for the Exploration of the Sea (ICES). The MARNET data from CMEMS (<https://doi.org/https://doi.org/10.48670/moi-00045>; <https://doi.org/https://doi.org/10.48670/moi-00032>) were subsampled to match the six-hour temporal resolution of the simulation results. Additional profile observations for the Baltic Sea were also obtained from ICES. We took occasional measurements and matched them in time and space with the simulation data.

We use satellite altimetry and gravimetry maps to obtain steric sea-level estimates from remote sensing. The altimetry data rely on multi-mission satellite retrievals merged to obtain optimal estimates of the sea-level anomaly (SLA) field in the global ocean. The sea-level anomaly field has a 25 km horizontal resolution and is available for free through the Copernicus Marine Environment and Monitoring Service (CMEMS 2022). The GRACE mission lasted for 14 years, from 2003 to 2016, which overlaps with the numerical experiments conducted in this study. We use the GRACE gravimetry gridded data from the Goddard Space Flight Center. The data is available as monthly averaged equivalent height of sea level, corrected for atmospheric pressure and glacial isostatic adjustment (GIA; Geruo et al. 2013). It is interpolated over a regular grid at a 50 km horizontal resolution (Loomis et al. 2019). The data is distributed through a dedicated web-portal at the Goddard Space Flight Center (<https://earth.gsfc.nasa.gov/geo/data/grace-mascons>).

2.3 Experimental design

This section describes the design of the experiments conducted to investigate the impact of wave-induced processes on thermosteric sea-level variability. The first experiment, referred to as EXP_{ref}, was performed over a 26-year period (1992–2017) using NEMO. It neglected the interaction of wave-induced forcings with the ocean circulation. An experiment was conducted to evaluate the sea-state contribution. The experiment, referred to as EXP_w, was performed over the same period as EXP_{ref} and used an ocean-wave coupled configuration with all WIPs activated (see Appendix 2 for more details). To ensure consistent results and accurately quantify the sea-state contribution to thermosteric sea-level, the same initial conditions were used in both EXP_{ref} and EXP_w. In 1992, the model's numerical simulations began with a 'cold start' (e.g. Bessières et al. 2017). The model provided only Temperature (T) and Salinity (S) fields. The

initial T and S fields for the Atlantic and the North Sea were obtained from the CMEMS GLORYS (19992–2009) and FOAM AMM7 (2010–2017) model outputs used for BDY forcing (O'Dea et al. 2012; Lellouche et al. 2018). The data for the Danish Straits and Baltic Sea were obtained from the CMEMS Baltic Sea ocean reanalysis dataset (Hordoir et al. 2015; Pemberton et al. 2017). Both datasets are tri-linearly interpolated on the GCOAST model grid.

The experiments differ solely because of the wave-coupling considered in EXP_w, so the different ocean and thermosteric sea-level variability obtained in the numerical integrations (see Sect. 3) are due to the effect of WIPs. The experimental set-up used in this study is detailed in Table 1.

2.4 Thermosteric sea level

Following the formulation of the sea-level balance in (Storto et al. 2019), the thermosteric sea level (η_t) can be expressed by computing the density anomaly at constant time-averaged salinity (S^*), i.e.:

$$\eta_t = -\frac{1}{\rho_0} \int_{\eta=-h}^{\eta=0} \delta\rho(T, S^*) dz \quad (1)$$

assuming that the effect of pressure on the steric sea-level anomalies can be considered negligible and is not considered in Eq. 1. In this study, the thermosteric sea-level anomalies were obtained from each experiment by considering three-dimensional temperature as daily averages and integrating over different vertical layers (0–150 m, 0–300 m, 0–700 m) to investigate the sensitivity of the thermosteric sea-level signal temporal evolution to the depth range considered. While this study focuses on the impact of wave-induced processes on thermosteric sea-level, the total steric sea-level (Eq. 1) signal emerging from each experiment was also

Table 1 The rows show the names of the relevant experiments, whereas the columns, from 1 to 4, detail the time window, atmospheric forcings (ATM), boundary conditions (BDC) and whether Ocean-Wave coupling was considered in the experiments. Note that Ocean-Wave coupling stands for the combined effect of wave-induced processes: Stoke-Coriolis forcings, sea-state-dependent momentum and energy fluxes. The same Time window, ATM and BDC apply to both experiments

	Time window	ATM	BDC	Ocean-Wave
EXP _{ref}	1992–2017	ERA5 (Hersbach et al. 2020)	AMM7 (O'Dea et al. 2012) GLORYS (Lellouche et al. 2018)	NO
EXP _w	Same	Same	Same	YES

computed to compare the results with altimetry-based steric sea-level estimates over the GCOAST domain (Sect. 3.1).

3 Results

In this section we assess the synergy of the numerical experiments with observations and the impact of WIPs on the ocean variability, thermosteric and steric sea-level. The results are based on a number of metrics detailed in Appendix 1.

3.1 Synergy with in-situ measurements and remote-sensing retrievals

Steric sea-level variability is driven by anomalies in the ocean density, which in turn rely on the vertical profile of

temperature and salinity that regionally can show large gradients enhancing significant departures from global steric sea-level, e.g. due to heat and salt transports (Stammer et al. 2013). Recent studies have shown that wave-induced processes contribute to vertical mixing in the ocean. This can modify temperature and salinity profiles (Alari et al. 2016; Stanev et al. 2019) as well as the thickness of the mixed layer. Therefore, it is important to assess the reference and wave-coupled experiments against the in-situ vertical profiles available over the GCOAST domain during the time window considered in this study. Figure 2 displays the changes in Temperature profiles over time. The in-situ observations at the German Bight (UFS Deutsche Bucht weather station) are compared with the outputs of the reference and wave-coupled experiment at the observation position (depicted by the red dots in the inlets). The observational records are displayed as colored dots in the panels, while

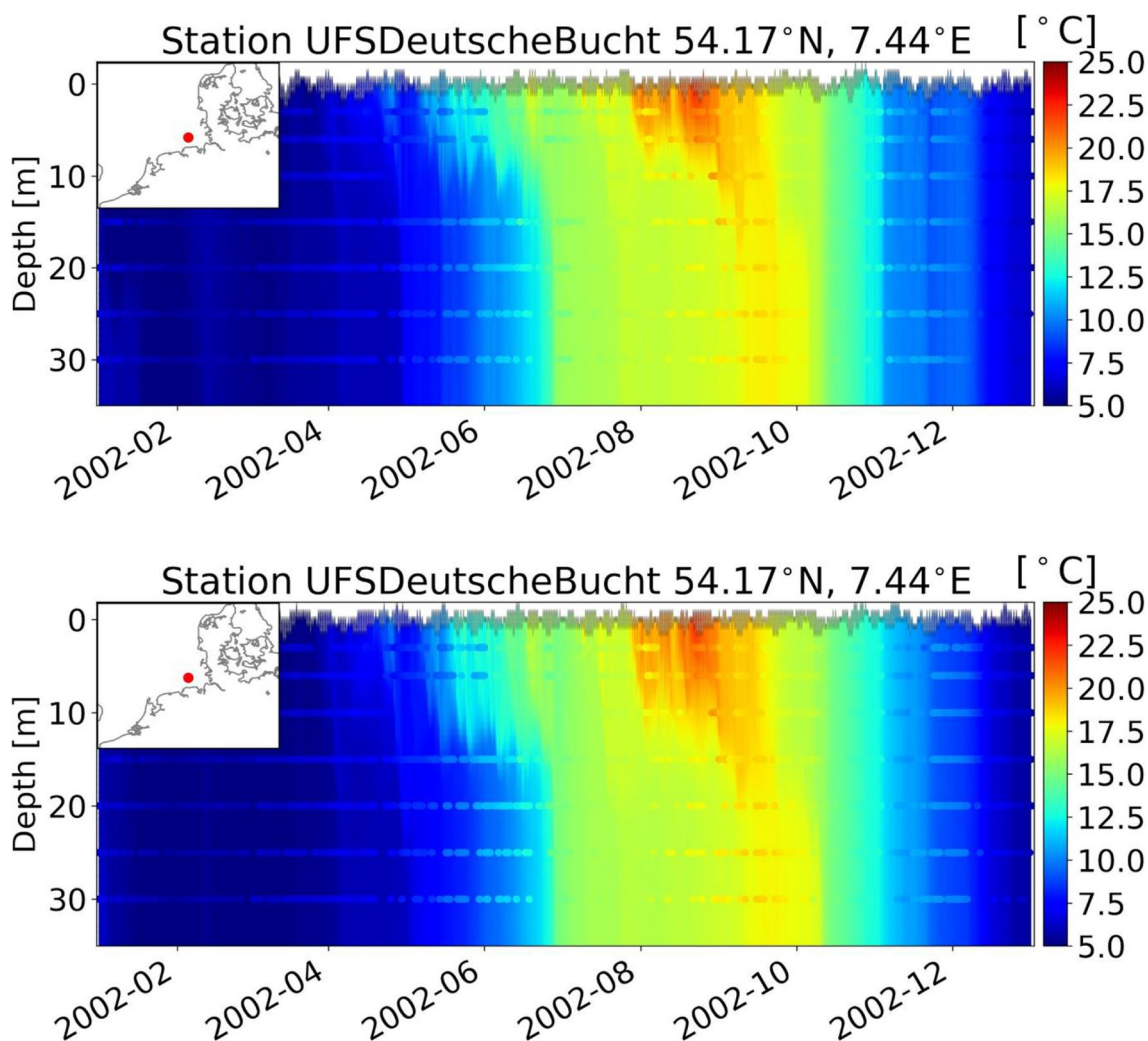


Fig. 2 Comparison between observed and simulated Temperature vertical profiles in the German Bight (map in the frame). The wave-coupled (top panel) and reference simulations (bottom panel) were considered at the observation position (red dots) over a 1-year period (2002)

the model outputs are shown in the background. Large differences between numerical results and observations can be identified as discontinuities in the Temperature field. These discontinuities tend to disappear as the differences become smaller. The model was enhanced by the ocean-wave coupling, which reduced vertical mixing. This effect is noticeable in the ocean temperature from April to October. The differences between the observed and simulated data tend to be smaller in the ocean-wave coupled experiment compared to the reference. Wave-induced mixing is most noticeable in the post-summer period when the water column is well stratified. The results demonstrate the impact of wave-induced forcing, or a combination of factors, on the vertical structure of stratification. These changes can occur rapidly in specific locations. Similar results were also obtained when comparing model outputs with observations during different years (i.e. 2008 and 2016; see Figure 11 and Figure 12).

The results of the different experiments were compared with remotely sensed estimates of steric sea level to assess the agreement with observations over the entire GCOAST spatial domain. The steric sea-level was calculated by subtracting the total and mass component sea-level signals obtained from satellite altimetry and gravimetry. The two signals combine to create the steric sea-level variability. This has been measured using the resultant and is also used to determine the ocean heat content globally. In this paper, we utilize the satellite altimetry and gravimetry synergy to evaluate numerical experiments from 2003–2016, the lifetime of the GRACE mission. When comparing various remote-sensing missions, satellite gravimetry solutions were used as data that had been corrected for mean atmospheric mass over the global ocean, which is consistent with IB-corrected

SLA from altimetry (Loomis et al. 2019). Satellite altimetry maps were sampled (binned) over the satellite gravimetry grid (see Sect. 2), taking into account monthly averaged fields. The pre-processing of numerical experiment results before comparing them with altimetry-based steric sea-level should also follow this rule. Figure 3 displays the variance of the sea-level anomaly (SLA) field obtained from altimetry maps over the GCOAST domain between 2003 and 2016. The sea-level anomaly field's variance reduction due to the mass component of sea-level variability is also presented in the results. This is done by taking into account the residual between altimetry and gravimetry retrievals, which is known as altimetry-based steric sea-level. The sea-level mass component is more noticeable over the shelf areas in the North Sea and Baltic Sea, but it decreases significantly in the open ocean, such as the Atlantic. Recent studies (Tinker et al. 2020) have found that steric sea-level explains a large portion of variability in the open ocean. These results will be used as a reference to evaluate the outcomes of numerical experiments in areas where steric sea-level variability is most prominent.

Figure 4 shows the root mean square error (RMSE) between the altimetry-based steric sea-level and the corresponding signal in the reference experiment. The North Sea, Baltic Sea, and Bay of Biscay exhibit large RMSE values, up to 6 cm, while smaller errors are noticeable in the Atlantic Ocean, such as the North Atlantic Drift. To evaluate the impact of sea-state on monthly steric sea-level variability, we also present the error reduction (ER*) as a percentage in the wave-coupled simulation compared to the reference experiments. Please refer to Appendix 1 for more information. An ER* value of 50% indicates that

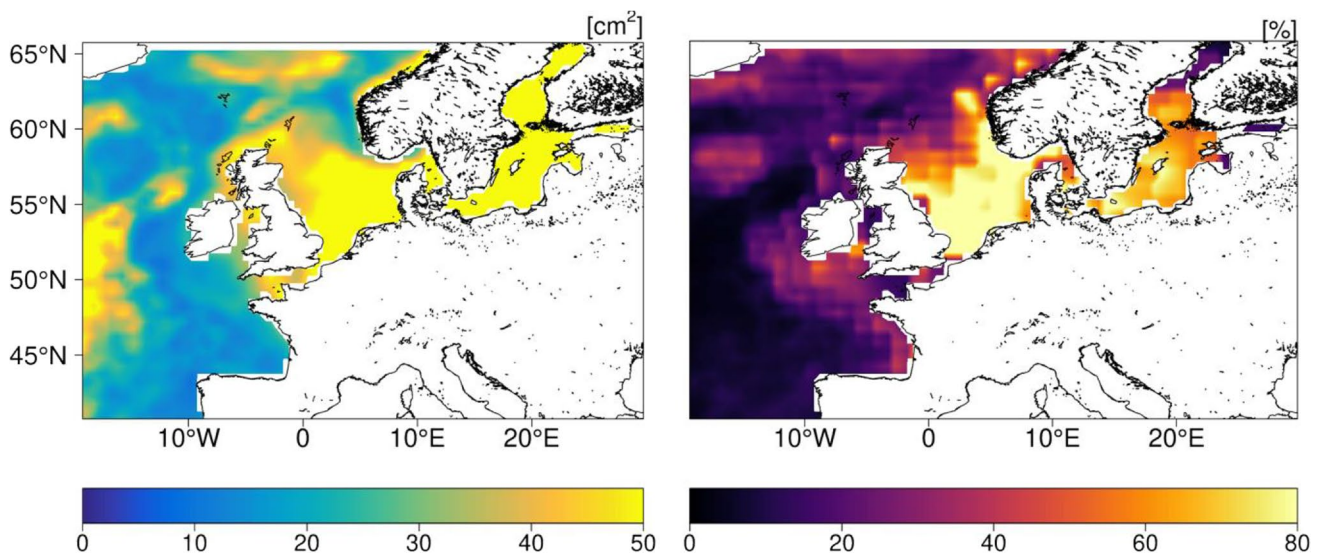


Fig. 3 Remote-sensed sea-level variability. Left Panel: sea-level anomaly variance (cm^2) over the period covered by the GRACE mission (2003–2016). Right panel: sea-level anomaly variance reduction (%) due to the mass component of variability

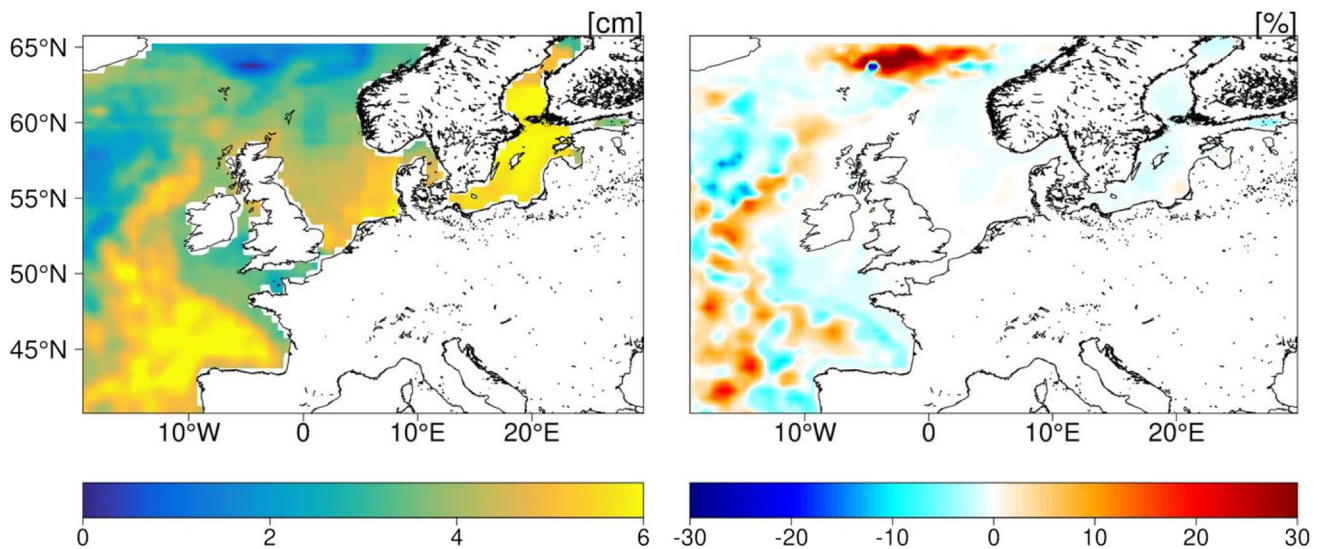


Fig. 4 Steric sea-level error reduction due to the effect of wave-induced processes. Left Panel: RMSE (cm) between altimetry-based steric sea-level and the reference experiment over the period covered by the GRACE mission (2003–2016). Right panel: RMSE reduction (ER*) in the wave-coupled simulation compared to the reference experiment, expressed as a percentage (%) of the altimetry-based steric sea-level standard deviation

the error in the wave-coupled experiment has reduced by half compared to the reference experiment. The results show that wave-coupling has a significant effect on the Atlantic, Bay of Biscay, and Norwegian Sea near the continental shelf break, resulting in an ER increase of up to 30%. However, the impact is much smaller on the extended continental shelf areas in the North Sea, where the steric sea-level only explains a small portion of the total sea-level signal. Tinker et al. (2020) found that shelf loading is the main cause of sea-level variability in these areas, while steric sea-level contributes significantly to the signal in the open ocean. The study suggests that wave-induced processes at the continental shelf break can modulate the influence of the open ocean on sea-level variability over shelf regions and play a role in the transition between dominant processes.

3.2 Sea-state contributions to ocean variability

The wind forcing is directly responsible for surface waves and drives ocean circulation. Therefore, we first examine the seasonal average of the wind from 1992 to 2017. It is evident that the wind is relatively calm during summer, with a magnitude of less than 3.5 m/s in almost all regions. During winter, the wind is stronger in the North Sea (with predominant direction from west to southwest, e.g. Sušelj et al. 2010), Norwegian Sea, and particularly in the Atlantic Ocean where seasonally averaged wind speeds of up to 5.7 m/s are found (Fig. 5). The stronger wind in the winter generates higher waves, resulting in differences in larger variability between the coupled and uncoupled experiments. During this season, the wind direction is controlled by the passage of extra-tropical cyclones that can be seen

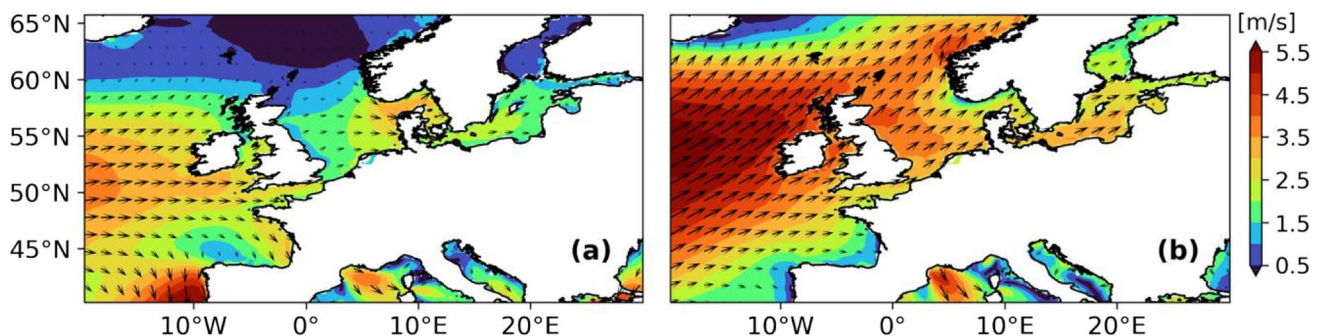


Fig. 5 Mean wind velocity during summer (left panel) and winter (right panel) over the period 1992–2017

to form jet clusters (Madonna et al. 2017). Recently, these clusters were found to be associated with specific sea-level patterns in Northern Europe (Mangini et al. 2021).

In the following part, this section examines how ocean-wave coupling affects various ocean variables. The differences between the reference and wave-coupled experiments during winter (DJF) and summer (JJA) are shown in Fig. 6

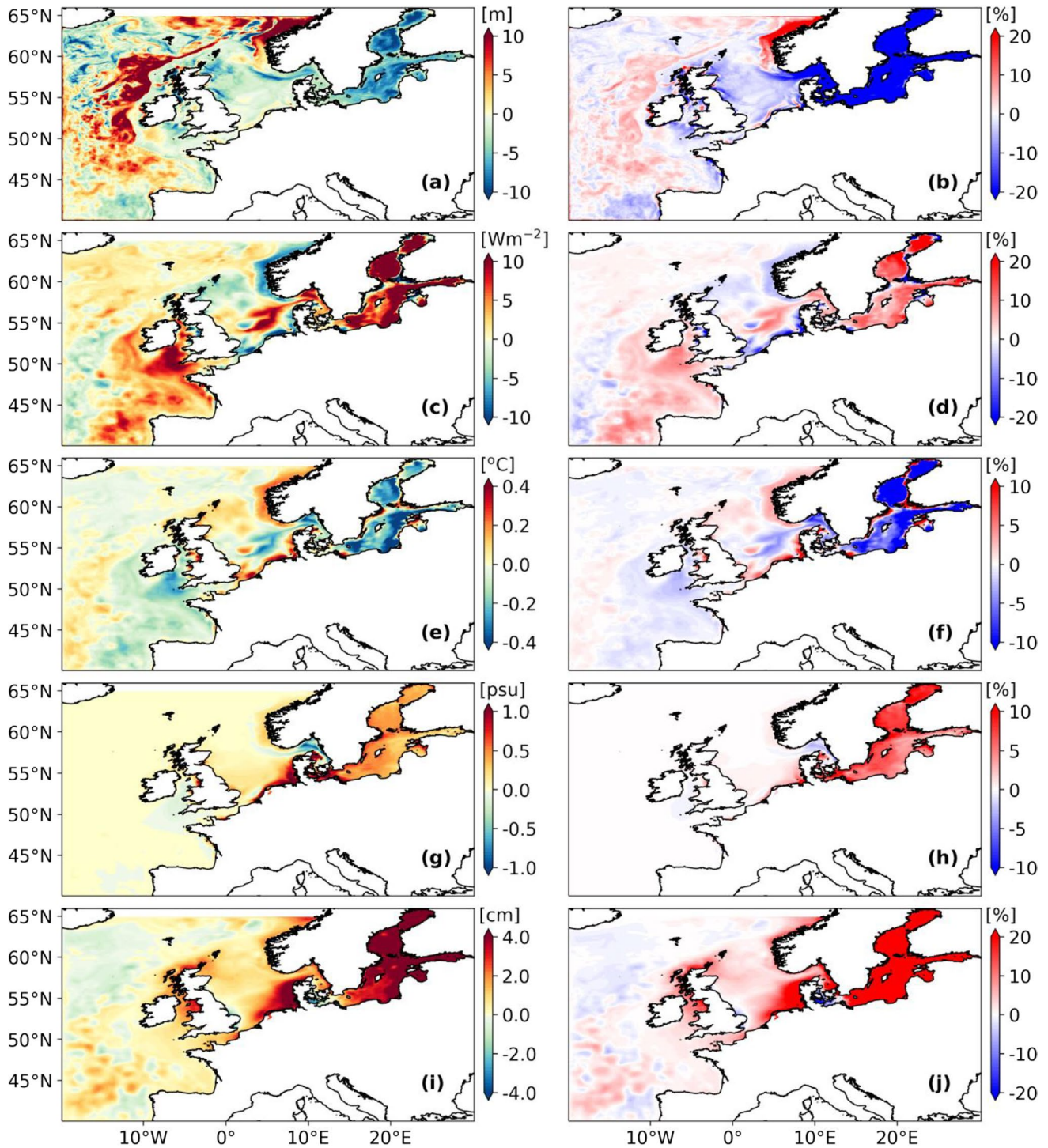


Fig. 6 Mean mixed layer depth (a, b), heat fluxes (c, d), sea-surface temperature (e, f), sea-surface salinity (g, h) and sea-surface height (i, j) differences (left panels) and normalized differences (%; right panels) between the wave-coupled (EXPw) and reference (EXPref) experiments over the period 1992 – 2017, during winter (DJF). Difference values unit shown in the (left) panels

and Fig. 7, respectively. Wave-induced processes have a direct impact on ocean circulation, which can be observed up to the MLD (Breivik et al. 2015). In the experimental set-up used in this study the MLD, computed by the NEMO model, is defined by the depth at which the density difference with the surface exceeds 0.01 kg m^{-3} (de Boyer Montégut et al. 2004). During winter, wave-induced processes deepen the MLD and cause differences of over 10 m in the Atlantic, Norwegian trench, and Norwegian coasts compared to the reference. Conversely, the North Sea and Baltic Sea experience the opposite scenario during winter, and the entire GCOAST domain experiences it during summer, albeit with

a lower magnitude of up to 3 m. The Figures also show the relative difference (RD) between the wave-coupled and reference experiments (right panel). RD is defined in Appendix 1. A positive (negative) RD indicates that the averaged signals in the wave-coupled experiment are larger (smaller) than those in the reference (EXPref). During summer, the RD consistently displays negative values exceeding 20% across all areas. This indicates that wave-modified mixing causes the MLD to become shallower during this season (not shown). In winter, strong winds over the Atlantic and North Sea can create high waves. This leads to large positive RD values along the Norwegian trench (20%) and in the

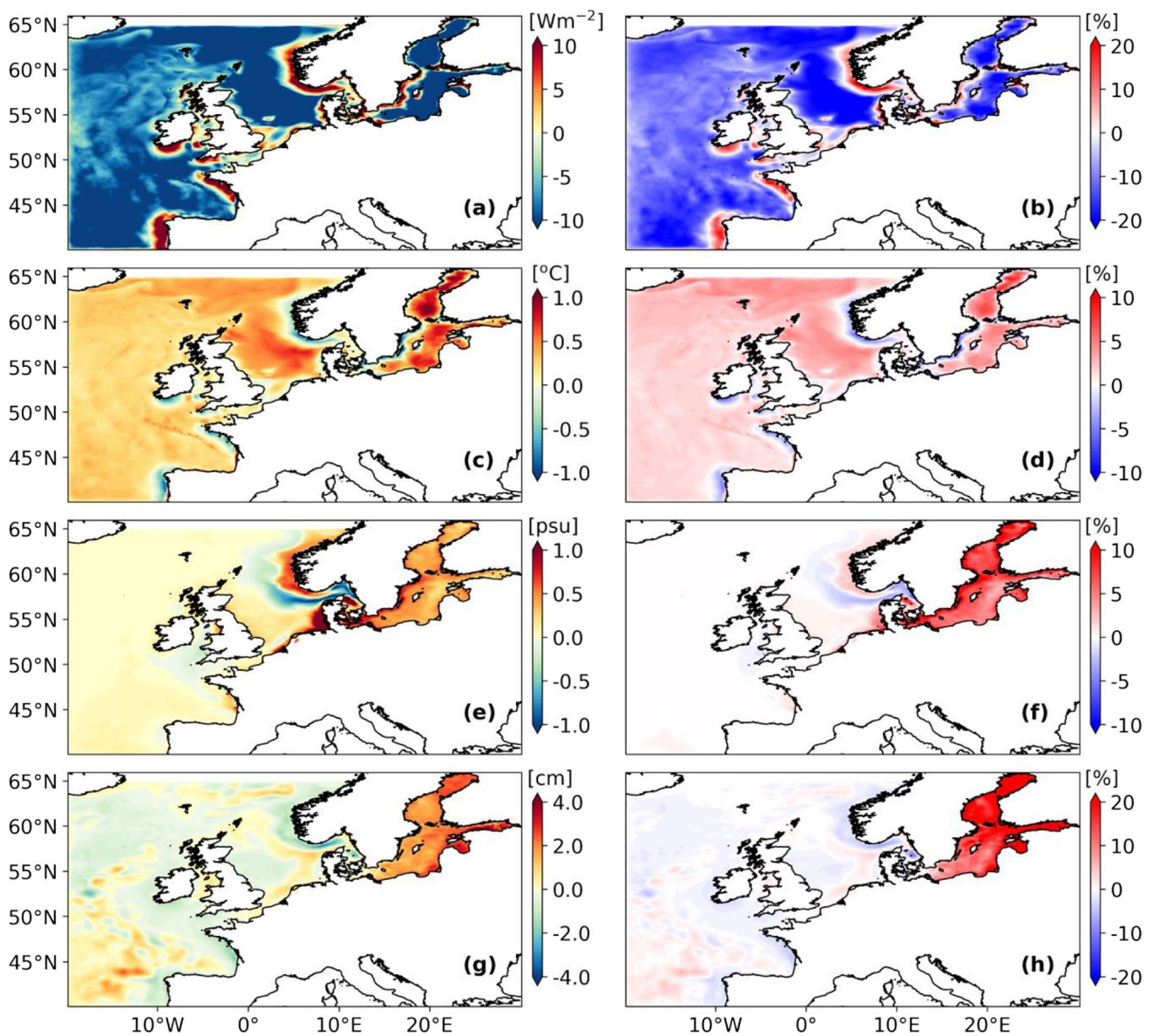


Fig. 7 Mean heat fluxes (a, b), sea-surface temperature (c, d), sea-surface salinity (e, f) and sea-surface height (g, h) differences (left panels) and normalized differences (%; right panels) between the wave-coupled (EXPw) and reference (EXPref) experiments over the period 1992 – 2017, during summer (JJA)

Atlantic Drift (up to 10%). This shows the importance of wave interactions with ocean currents in these areas. Negative RD values ($> 20\%$) were observed in the North Sea and Baltic Sea during the same season.

Steric sea-level is a reliable indicator of the heat stored in the ocean (Meyssignac et al. 2019). The interaction between the atmosphere and the ocean is influenced by wave-induced processes (e.g. Breivik et al. 2019). Therefore, it is informative to examine the differences in the experiments in terms of heat fluxes towards the ocean. In the Figures, positive (negative) values indicate larger (smaller) heat fluxes from the atmosphere to the ocean in the ocean-wave coupled experiment. During the summer, the ocean tends to store heat from the atmosphere. However, wave-modified processes can modulate this tendency, such as wave-modified roughness and sea-state modified momentum fluxes (as discussed in Alari et al. 2016). As a result, negative RD values were observed over the GCOAST domain, except in coastal areas characterized by coastal upwelling (as noted in Wu et al. 2019), where wave-modified vertical mixing may play a role. During winter, the coupling between the ocean and waves alters the interaction between the ocean and atmosphere, resulting in a reduction of ocean heat loss (positive RDs), except the Norwegian Trench.

As anticipated, the variations in ocean–atmosphere heat fluxes are reflected in the SST patterns in both experiments, with differences greater than $1\text{ }^{\circ}\text{C}$ due to wave-induced forcings during summer, as shown in Fig. 8. Specifically,

ocean-wave coupling in EXPw tends to increase (reduce) SST during summer (winter) by more than 10% compared to the reference. This is in line with the findings of Alari et al. (2016). The authors investigated the effect of surface waves on water temperature through ocean-wave coupled experiments and found wave-induced positive differences in the Baltic Sea during the same season due to wave coupling. They argued that the warming was related to wave-induced energy fluxes. The authors also observed a wave-induced cooling in near-coastal areas due to intensified upwelling triggered by Stokes–Coriolis forcings. This study's findings are consistent with wave-induced differences observed during summer in coastal areas over the GCOAST domain, which is characterized by upwelling systems such as the Norwegian Trench and North West Iberian Coast (Winther and Johannessen 2006; Pitcher et al. 2010; Christensen et al. 2018). During winter, the SST values in the reference tend to be larger compared to the wave-coupled experiment, highlighting the effect of waves on vertical mixing. This effect can be poorly represented if wave-induced processes are neglected, as shown in Fig. 2.

When considering SSS, the largest differences ($> 1\text{ psu}$) were observed in the area of the German Bight estuaries. This was due to ocean-wave coupling, which induced positive anomalies compared to the reference (Stanev et al. 2019). This is consistent with the findings of (Schloen et al. 2017), who investigated wave-current interactions in the southern North Sea. They suggested that wind waves tend to weaken estuarine circulation, thereby increasing the net transport of ocean

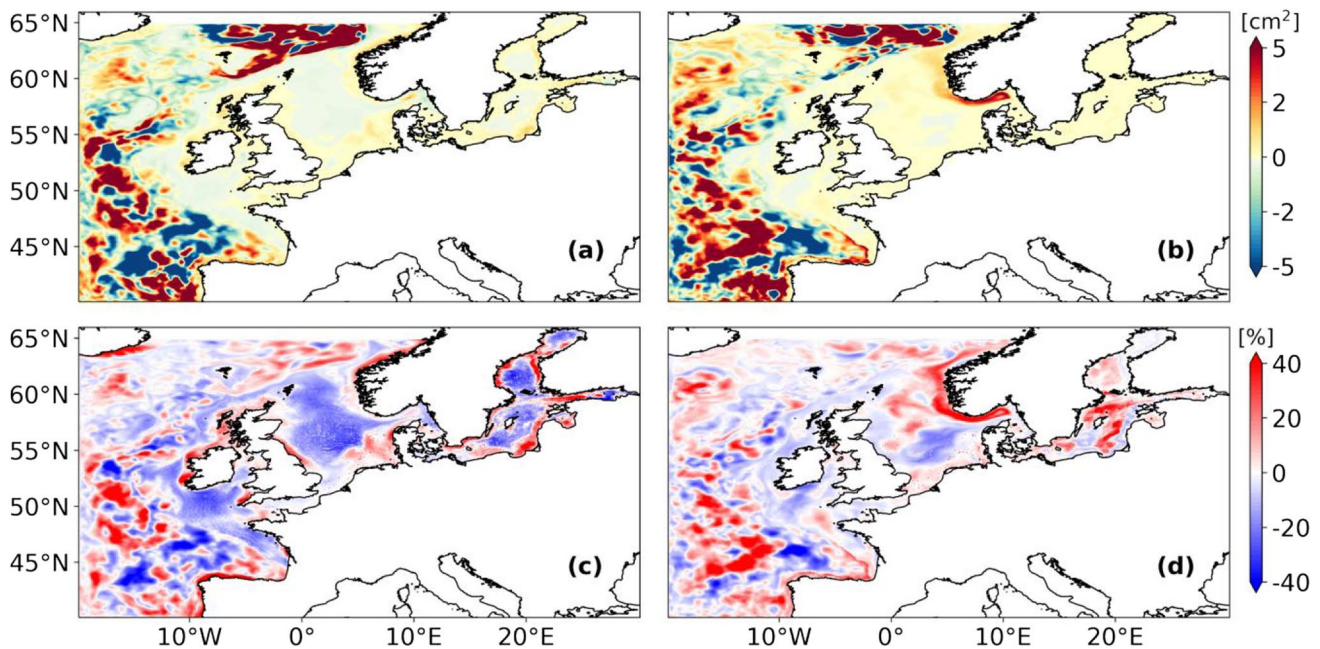


Fig. 8 Seasonal differences of variances (cm^2) of thermosteric sea-level during summer (JJA; left panels) and winter (DJF; right panels) over the period 1992 – 2017 integrated from sea surface to 700 m depth. The bottom panels show the results relative to the variance of the signal in the reference experiment (VAR^* ; %)

water towards the coast. The authors also observed positive salinity anomalies at the surface, propagating from the coastal zone towards the open ocean, similar to the SSS differences observed in the current study. In the Baltic Sea, RD was found to be positive (10%) during both winter and summer. The pattern of SSS differences in the Norwegian Trench reflects those observed in the HF and SST fields. During summer, colder temperatures are associated with saltier waters, while warmer temperatures are associated with fresher waters. The area exhibits a distinct separation between positive and negative wave-induced differences, highlighting the impact of ocean-wave coupling on the modulation of Atlantic water transformation. This effect, however, does not extend to the North Sea (Winther and Johannessen 2006).

The wave-induced processes clearly show their signature in the expression of the sea-surface height. The contributions were larger than 3 cm (RD > 10%) during the winter in the German Bight and in the Baltic Sea. This was in line with the findings of Bonaduce et al. 2020 who, looking at sea-level extremes, found that sea-state contributions play a significant role over the shelf due to wave-modified momentum fluxes, and in the open ocean where the combined effect of wave-modified momentum and energy fluxes and vertical mixing modulate the sea-level variability, in particular at the shelf break. The latter was also observed in the current study, e.g. in the Bay of Biscay and North Atlantic Drift, considering results over more than two decades.

The results presented in this section show how the effect of ocean waves can modulate the fluxes between ocean and atmosphere (e.g. HF), and their effect on ocean circulation can be noticed at the surface and at depth (e.g. MLD in winter). In the next section, we focus on the effect of wave-induced processes on thermosteric sea-level obtained from the numerical model outputs in each experiment.

3.3 Sea-state contribution to thermosteric sea-level variability

In this Section we compare the results obtained in the numerical experiments to assess the contribution of WIPs to thermosteric sea-level variability over the GCOAST domain.

Following the approach proposed by Storto et al 2019, thermosteric sea-level was computed post-processing the three-dimensional temperature fields in the numerical experiments, as detailed in Sect. 2. To evaluate the differences between the experiments in terms of thermosteric sea-level variability we considered the relative variance (VAR^* ; see Appendix 1) to assess how wave-induced processes enhance differences in the representation of thermosteric sea-level among the experiments relative to the variance of the signal in EXP_{ref} .

The thermosteric sea-level signals were obtained considering different depth ranges: 150, 300, 700 m. The maximum depth range between 0–700 m was defined following the

approach typically proposed by other authors in the literature to account for heat content in the upper ocean and steric sea-level (Levitus et al. 2009; Lyman and Johnson 2014; Palmer et al. 2017; Storto et al. 2017, 2019; Meyssignac et al. 2019).

Figure 8 shows the results of the comparison of the 0–700 m thermosteric sea level obtained in each experiment. The panels show the variance of the differences between the experiments during winter and summer. The largest values ($> 5 \text{ cm}^2$) were observed in the deepest areas over the GCOAST domain, including the Bay of Biscay, the North Atlantic Drift, and the area of Norwegian-Atlantic slope and front currents. In these areas, the experiments show that waves play a significant role in modifying the vertical structure of Atlantic waters along their pathways across the European shelf and towards the northern high latitudes, resulting in differences in the thermosteric sea-level signals. These differences exhibit spatial patterns associated with mesoscale features of the ocean circulation, as observed by Bonaduce et al. (2020), who investigated the combined effect of wave-modified surface stress and vertical mixing, for example, in the North Atlantic Drift. The VAR^* (right panels) enabled the distinction of the contribution to thermosteric sea-level variability over the shelf areas in the North Sea and the Baltic. In the North Sea, ocean waves tend to reduce the MLD and modify the transport of Atlantic waters that enter the North Sea through the Orkney-Shetland section during summer. The combined effect of these changes reduces the thermosteric sea-level over the shelf. During winter, a more complex pattern can be observed in the same area. The VAR^* values were up to 40% in the Atlantic (southern part of the GCOAST domain). Fine-scale differences are observable along the continental slope in the Bay of Biscay and the Atlantic Drift. Positive values of approximately 30% are present in the Baltic and along the Norwegian Trench. These values may be attributed to the effect of Stokes-Coriolis forcing in those areas, as discovered by Alari et al. 2016.

The previous results (i.e. Figure 8) indicate significant contributions from sea-state to thermosteric sea-level in the North Atlantic and Norwegian Sea. When investigating the temporal evolution of the thermosteric sea-level in these regions, differences up to an order of $> 1 \text{ cm}$ were observed due to ocean-wave coupling. Figure 9 illustrates the differences between the experiments based on the depth range used to compute the thermosteric sea-level signal. In the North Atlantic, the largest differences were observed for a depth range of 0–700 m in 2016. Smaller variations were noticed for shallower ranges. It is worth noting that when considering the thermosteric sea-level up to a depth of 150 m, the results indicate positive differences that can exceed those obtained when considering a vertical layer down to 300 m during the 90 s. However, starting from the 2000s, the 0–300 m steric sea-level shows larger contributions compared to those obtained when considering shallower waters. In the deep areas of the Norwegian Sea, WIPs exhibit a pronounced signature even at depth, as observed in the temporal evolution of the 0–700 m thermosteric sea-level.

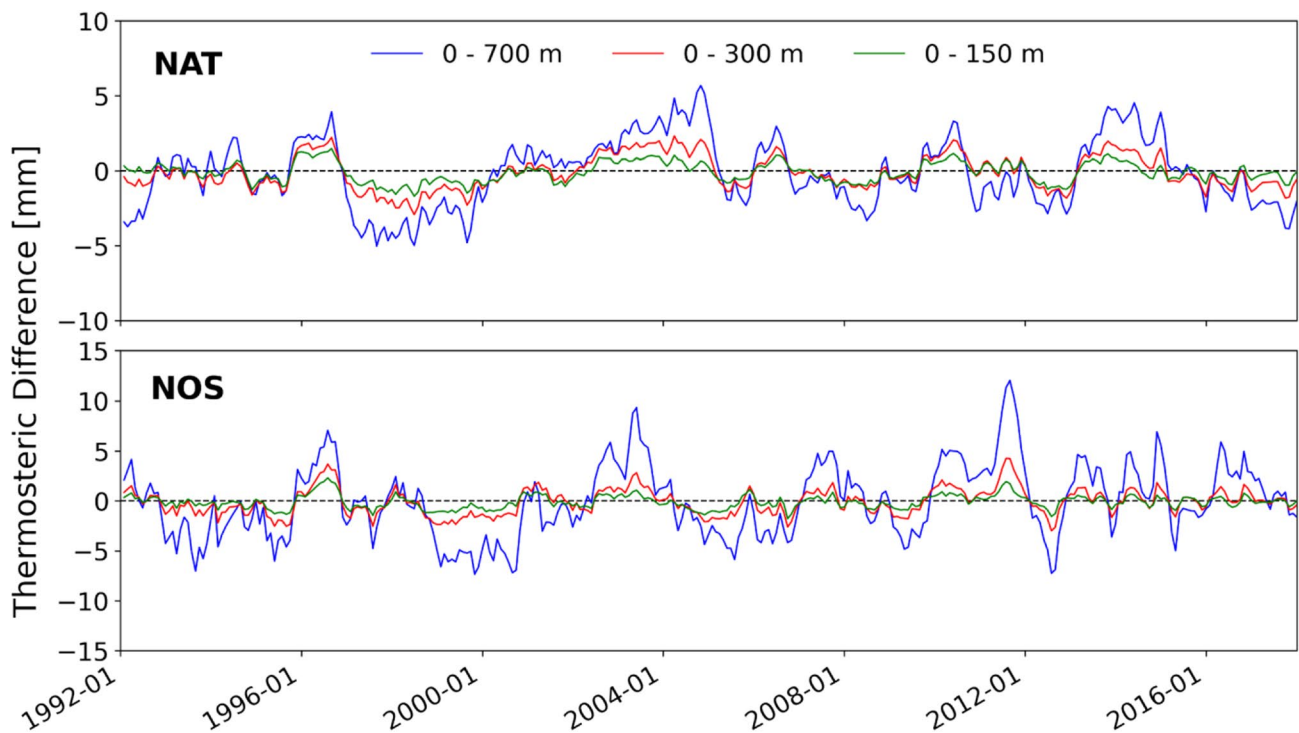


Fig. 9 Thermosteric sea-level differences between the experiments during the period 1992–2107 in the North Atlantic (top panel) and Norwegian Sea (bottom panel), as a function of depth ranges: 0–150 m (green lines), 0–300 m (red lines), 0–700 m (blue lines). Positive (negative) values stand for a larger (smaller) thermosteric sea-level in the wave-coupled simulation. Note the range of y-axis in the panels; values expressed as mm

3.4 Sea-state contribution to thermosteric sea-level trend

This section investigates the contribution of sea-state to thermosteric sea-level trends by comparing wave-coupled and reference experiments. A trend analysis was performed over the period covered by the numerical experiments, considering

the 0–700 m thermosteric sea-level. Figure 10 displays the signature of WIPs in the spatial variability of thermosteric sea-level trends. Significant differences of over 1 mm per year can be observed between the experiments during both summer and winter. The largest contributions to sea-state over the GCOAST domain are observed in areas where the steric sea-level explains a large portion of the total sea-level

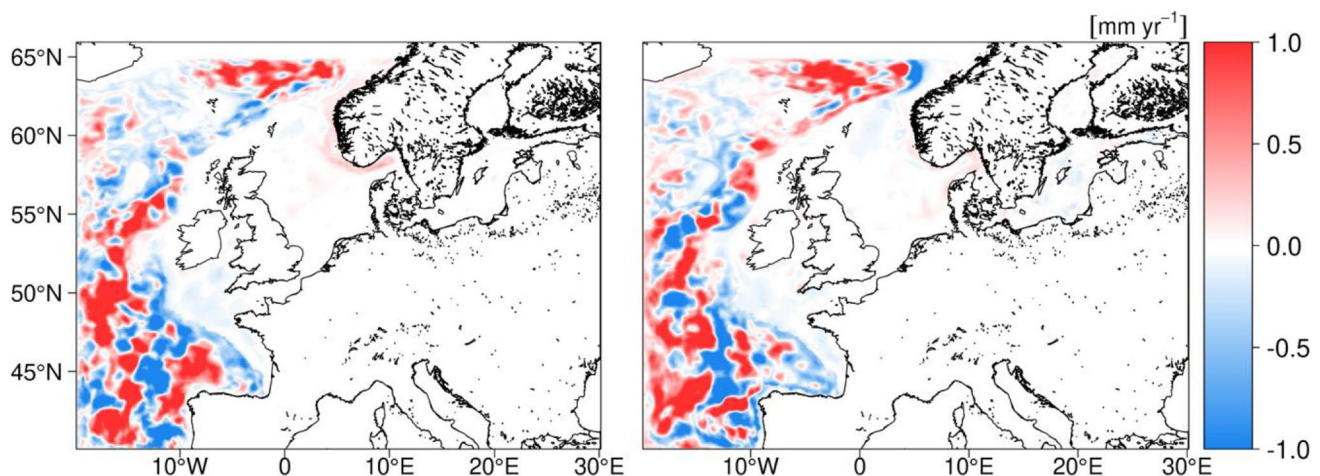


Fig. 10 Thermosteric sea-level (0–700 m) trend differences due wave-induced forcings over the period 1993–2017, during winter (DJF; right panels) and summer (JJA; left panels). Values expressed as mm yr^{-1}

variability, such as in the open ocean and along the continental slope. These results are consistent with those obtained from considering altimetry-based steric sea-level variability (Sect. 3.1). In these areas, wave-induced processes contribute to spatial scales associated with mesoscale dynamics, as found by Bonaduce et al. (2020) in their investigation of the sensitivity of non-tidal residuals to WIPs during extreme events. The authors discovered that this signature of wave-induced processes in the Atlantic is driven by the interaction of wave-modified momentum flux and turbulent mixing, while wave-induced energy fluxes may play a role at the shelf break. It is argued that the combination of wave-modified momentum and energy fluxes affects ocean dynamics and vertical mixing, which in turn alters the distribution of water masses and density structure. These changes are reflected in the thermosteric sea-level variability and trends, particularly in deep water areas beyond the continental slope.

4 Concluding discussion

The study investigated the impact of sea-state on thermosteric sea-level variability and trends using ocean-wave coupled simulations spanning 26 years (1993–2017). Two experiments were conducted: a reference experiment (EXP_{ref}) that excluded wave-induced processes, and a wave-coupled experiment (EXP_w) that considered wave-induced processes such as Stokes-Coriolis forcings, wave-modified momentum, and energy fluxes computed by the WAM model.

To investigate the effect of ocean-wave coupling on thermosteric sea-level variability and trends, we selected an analysis period of over two decades. We assessed the synergy of numerical experiments with observations by considering both in-situ measurements and remote-sensing retrievals. Compared to in-situ measurements, the GCOAST system was enhanced by ocean-wave coupling to more accurately mimic the temporal evolution of temperature and salinity profiles, particularly when waters are well stratified (e.g. after summer) due to wave-induced mixing, as shown in the reference experiment.

During the GRACE mission period (2003–2016), a study was conducted to investigate the correlation between steric sea-level estimates obtained from remote-sensing and the EXPs. The study found that wave-induced processes were evident at the continental shelf break, where there may be a decoupling between coastal and open ocean sea-level signals (Hughes et al. 2019). The study also observed a significant ER (up to 30%), suggesting a role of ocean waves in modulating the transition between dominant sea-level variability in the open ocean and over the continental shelf areas. The study results also indicate a significant influence of thermosteric sea-level in these areas.

The study compared numerical experiments to investigate the impact of ocean-wave coupling on ocean variability. The results showed that wave-induced processes contribute to sea

surface dynamics, ocean mixing (mixed layer thickness), and modulation of air-sea fluxes (e.g. heat flux) during both winter (10–20%) and summer (10%), which affects the steric sea-level signals. These results can also be applied to the differences in sea-surface height induced by waves, which are observable both in the open ocean and over shelf areas. This complements the previous findings of Bonaduce et al. (2020), who highlighted the contribution of sea-state to surges during extreme events and demonstrated the signature of wave-induced processes in SSH patterns of variability over more than two decades.

The North Atlantic had the largest sea-state contributions (up to 40%) to thermosteric sea-level in summer, while the Norwegian Sea and Norwegian Trench had the largest contributions in winter. These contributions are due to wave-modified momentum and energy fluxes, which affect the variability of thermosteric sea-level. WIPs have an impact on the thermosteric sea-level trends in the North Atlantic, up to approximately 1 mm yr⁻¹. This effect is observed during both winter and summer, in the open ocean and at the shelf break. However, smaller contributions are noted over the shelf areas. The results of the study highlight the impact of wave-modified momentum and energy fluxes on ocean dynamics and vertical mixing, which in turn affects the distribution of water masses and density structure, reflected in thermosteric sea level variability and trends. Particularly in deep water areas beyond the continental slope, where ocean density anomalies contribute significantly to the signal (Tinker et al. 2020).

The aim of this study was to assess the contribution of the ocean state to the thermosteric sea level variability and trend at a regional scale by performing high-resolution numerical experiments that are coupled to ocean waves. Future investigations based on ocean-wave coupled simulations should aim to evaluate these contributions at a global scale and their response to climate change drivers.

Appendix 1

Synergy with remote-sensing observations

In the comparison between the remote-sensing retrievals and numerical experiments (Sect. 3.1), the sea-state contributions to steric sea-level variability were assessed in terms of the error reduction ER*, expressed as a percentage, in the wave-coupled simulation compared to the reference experiments, where ER* is defined as

$$ER^* = 100 \times \frac{RMSE(EXP_{ref}) - RMSE(EXP_w)}{RMSE(EXP_{ref})}$$

where $RMSE(EXP_k)$ is the RMSE in k th experiments compared to the steric sea-level obtained from remote-sensing. A value 50% means that the error in the wave-coupled

experiment has halved with respect to the reference experiment.

Assessment of sea-state contributions to ocean variability

In order to assess the sea-state contributions of the ocean variability, the relative difference (RD) between the wave-coupled and reference experiments was considered defined as:

$$RD = 100 \times \frac{EXP_w - EXP_{ref}}{EXP_{ref}}$$

Positive (negative) values of RD mean that the averaged signals in the wave-coupled experiment (EXP_w) are larger (smaller) than those in the reference (EXP_{ref}).

Assessment of sea-state contribution to steric sea-level variability

In order to assess the differences between the experiments in terms of thermosteric sea-level variability we considered the relative variance, VAR^* , defined (in terms of percentage) as follows:

$$VAR^* = 100 \times \frac{\sigma_{diff}^2}{\sigma_{ref}^2}$$

where σ_{diff}^2 is the variance of the differences obtained by comparing EXP_w with EXP_{ref} (the reference experiment), and σ_{ref}^2 is the variance of the signals in the reference experiment.

Appendix 2

Wave-induced processes

The following paragraphs detail the wave-induced processes considered in the ocean-wave coupled experiment: Stokes-Coriolis forcing, sea-state-dependent momentum fluxes, sea-state-dependent energy fluxes.

Stokes-Coriolis forcing

Stokes drift refers to the drift in the direction of wave propagation induced by the motion of surface waves (Stokes 1847). Fluid particle trajectories in water waves are not perfectly circular, primarily due to the differing speeds of wave crests and troughs (e.g., Staneva et al. 2017). This discrepancy creates a difference between the average Lagrangian flow velocity of a fluid parcel and the Eulerian flow velocity, known as the Stokes drift. Similar to wave-induced currents, the Stokes drift is influenced by

the Earth's rotation, contributing additionally to ocean currents through the Stokes-Coriolis force (Hasselmann 1970):

$$\frac{Du}{Dt} = -\frac{1}{\rho} \nabla p + (u + v_s) \times f \hat{z} + \frac{1}{\rho} \frac{\partial \tau}{\partial z}$$

where v_s is the Stokes drift vector, p is the pressure, τ is the surface stress and \hat{z} is the upward unit vector.

The current implementation of ocean-wave coupling between the NEMO and WAM models in GCOAST also takes into account the effects of Stokes drift on tracer advection (such as temperature and salinity) and mass transport (e.g., Wu et al. 2019).

Sea-state-dependent momentum fluxes

The presence of waves significantly influences wind stress, especially during storms (e.g., Staneva et al. 2017). As waves grow, they absorb momentum from the atmosphere, reducing the stress felt by ocean currents. Conversely, when waves break, they release momentum back into the ocean. Consequently, the ocean-side stress, τ_{oc} , is defined as:

$$\tau_{oc} = \tau_a - \tau_{in} - \tau_{db}$$

where τ_a is the atmospheric stress, τ_{in} is momentum extracted by waves from the atmosphere as they grow, and τ_{db} is the momentum released by waves (negative) to the ocean as they mature and break.

Ocean-side stress balances the atmospheric stress only when the input of momentum by wind is balanced by the release of momentum through breaking (fully developed sea).

The momentum flux τ_{in} is enhanced through the variations of sea-surface roughness (z_0) as waves grow, which in turn is related to the friction velocity $u_*^2 = \frac{\tau_a}{\rho_a}$:

$$z_0 = \alpha CH \frac{u_*^2}{g}$$

where ρ_a is the air density, g is the acceleration due to gravity and αCH is known as the Charnock constant (Charnock 1955). Janssen (1989) assumed αCH not as a constant but as sea-state dependent:

$$\alpha CH = \frac{\hat{\alpha} CH}{\sqrt{1 - \tau_{in}/\tau_a}}$$

where $\hat{\alpha} CH = 0.006$ (see ECMWF 2019 for further details).

The sea-state-dependent roughness can be used to define the wave-modified drag coefficient:

$$C_D = \frac{k^2}{\log^2(10/z_0)}$$

where k is the von Kármán's constant.

The momentum flux going into NEMO from WAM depends on the wave-modified drag coefficient, which changes the air-side stress and the ocean-side stress, which, as already mentioned, depends on the balance between wave growth and dissipation (Staneva et al. 2017).

Sea-state-dependent energy fluxes

As waves break, they can introduce strong turbulence into the water column, especially during storms (e.g., Alari et al. 2016). Numerous studies have highlighted the significance of wave-generated and wave-induced turbulence both at the surface and at depth (Jones and Davies 1998; Davies et al. 2000; Babanin and Chalikov 2012).

In NEMO, the wave-induced turbulent kinetic energy (TKE) flux is influenced by the wave energy factor αCB (Craig and Banner 1994), which is treated as a constant value ($\alpha CB = 100$) representing an average between young and mature seas, regardless of the sea state. However, observations and numerical model-based studies have shown that αCB is not constant and actually varies with the sea state (Gerbi et al. 2009; Fan and Hwang 2017).

In this context, Alari et al. (2016) and Staneva et al. (2017), using the WAM spectral wave model, estimated the momentum flux from the breaking waves source term (Breivik et al. 2015) and demonstrated the variability of αCB in the North Sea and Baltic Sea. This approach was also utilized in the present study to account for sea-state-dependent energy fluxes.

Appendix 3

Synergy with in-situ observations

See Fig. 11 and Fig. 12.

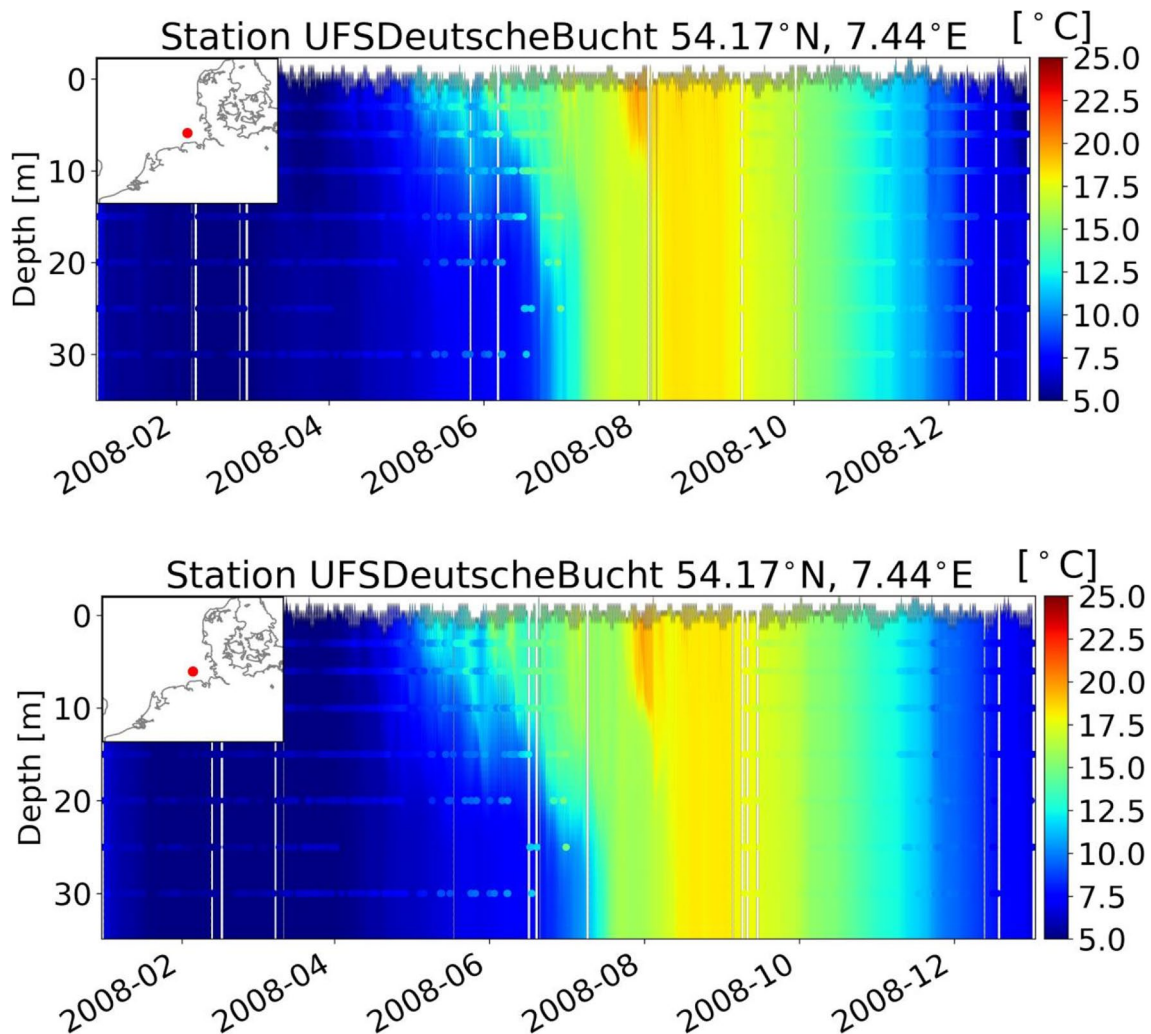


Fig. 11 As in Fig. 2, but considering Temperature vertical profiles during 2008

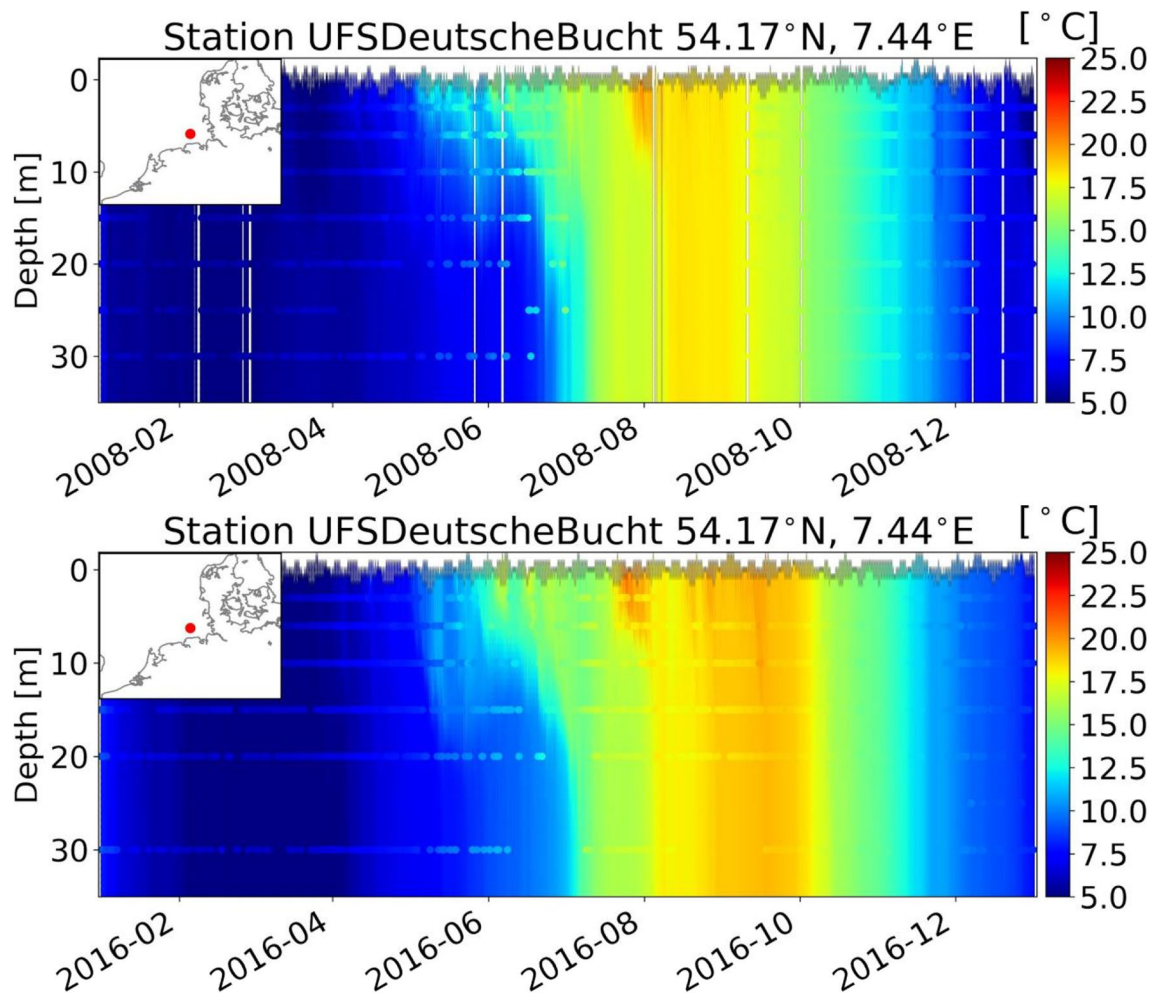


Fig. 12 As in Fig. 2, but considering Temperature vertical profiles during 2016

Acknowledgements The Initiative and Networking Fund of the Helmholtz Association supported the initial phase of the study through the project Advanced Earth System Modelling Capacity (ESM). The analyses were performed using the high performance computer at Helmholtz Zentrum Hereon and German Climate Computing Centre (DKRZ) JS receives funding from the European Union’s Horizon 2020 REST-COAST: Large scale restoration of coastal ecosystems through rivers to sea connectivity (grant agreement 101037097). JS and SG acknowledge Horizon Europe Project Edito Model lab (Grant Agreement 101093293). NP gratefully acknowledges the Helmholtz European Partnership project SEA-ReCap: Research Capacity Building for healthy, productive and resilient Seas and DOORS project (Grant Agreement 101000518). AB and RR were supported through the Sea Level Predictions and Reconstructions (SeaPR) Project funded by the Bjerknæs Center for Climate Research (BCCR) initiative for strategic projects. ØB gratefully acknowledges funding from the Research Council of Norway through the ENTIRE project (grant no 324227).

Funding Open Access funding enabled and organized by Projekt DEAL.

Open Access This article is licensed under a Creative Commons Attribution 4.0 International License, which permits use, sharing, adaptation, distribution and reproduction in any medium or format, as long

as you give appropriate credit to the original author(s) and the source, provide a link to the Creative Commons licence, and indicate if changes were made. The images or other third party material in this article are included in the article’s Creative Commons licence, unless indicated otherwise in a credit line to the material. If material is not included in the article’s Creative Commons licence and your intended use is not permitted by statutory regulation or exceeds the permitted use, you will need to obtain permission directly from the copyright holder. To view a copy of this licence, visit <http://creativecommons.org/licenses/by/4.0/>.

References

- Alari V, Staneva J, Breivik Ø, Bidlot J-R, Mogensen K, Janssen P (2016) Surface wave effects on water temperature in the Baltic Sea: simulations with the coupled NEMO-WAM model. *Ocean Dyn* 66:917–930. <https://doi.org/10.1007/s10236-016-0963-x>
- Arns A, Dangendorf S, Jensen J, Talke S, Bender J, Pattiaratchi C (2017) Sea-level rise induced amplification of coastal protection design heights. *Sci Rep* 7:40171. <https://doi.org/10.1038/srep40171>
- Babanin AV, Chalikov D (2012) Numerical investigation of turbulence generation in non-breaking potential waves. *J Geophys Res Oceans* 117. <https://doi.org/10.1029/2012JC007929>

- Bessi eres L, Leroux S, Brankart J-M, Molines J-M, Moine M-P, Bouttier P-A et al (2017) Development of a probabilistic ocean modelling system based on NEMO 3.5: application at eddy resolution. *Geosci Model Dev* 10:1091–1106. <https://doi.org/10.5194/gmd-10-1091-2017>
- Bindoff NL, Willebrand J, Artale V, Cazenave A, Gregory J, Gulev S, Hanawa K, Le Qu er e C, Levitus S, Nojiri Y, Shum CK, Talley LD, Unnikrishnan A (2007) Observations: Oceanic Climate Change and Sea Level. In: Solomon S, Qin D, Manning M, Chen Z, Marquis M, Averyt KB, Tignor M, Miller HL (eds.) *Climate Change 2007: The Physical Science Basis. Contribution of Working Group I to the Fourth Assessment Report of the Intergovernmental Panel on Climate Change*. Cambridge University Press, Cambridge, United Kingdom and New York, NY, USA
- Bonaduce A, Pinardi N, Oddo P, Spada G, Larnicol G (2016) Sea-level variability in the Mediterranean Sea from altimetry and tide gauges. *Clim Dyn* 47:2851–2866. <https://doi.org/10.1007/s00382-016-3001-2>
- Bonaduce A, Staneva J, Behrens A, Bidlot J-R, Wilcke RAI (2019) Wave Climate Change in the North Sea and Baltic Sea. *J Mar Sci Eng* 7:166. <https://doi.org/10.3390/jmse7060166>
- Bonaduce A, Staneva J, Grayek S, Bidlot J-R, Breivik   (2020) Sea-state contributions to sea-level variability in the European Seas. *Ocean Dyn* 70:1547–1569. <https://doi.org/10.1007/s10236-020-01404-1>
- Breivik  , Carrasco A, Staneva J, Behrens A, Semedo A, Bidlot J-R, et al. (2019) Global Stokes Drift Climate under the RCP8.5 Scenario. <https://doi.org/10.1175/JCLI-D-18-0435.1>
- Breivik  , Mogensen K, Bidlot J-R, Balmaseda MA, Janssen PAEM (2015) Surface wave effects in the NEMO ocean model: Forced and coupled experiments. *J Geophys Res Oceans* 120:2973–2992. <https://doi.org/10.1002/2014JC010565>
- Cazenave A, Remy F (2011) Sea level and climate: measurements and causes of changes. *Wires Clim Change* 2:647–662. <https://doi.org/10.1002/wcc.139>
- Chaigneau AA, Reffray G, Voldoire A, Melet A (2022) IBI-CCS: a regional high-resolution model to simulate sea level in western Europe. *Geosci Model Dev* 15:2035–2062. <https://doi.org/10.5194/gmd-15-2035-2022>
- Charnock H (1955) Wind stress on a water surface. *Q J R Meteorol Soc* 81:639–640. <https://doi.org/10.1002/qj.49708135027>
- Chen W, Schulz-Stellenfleth J, Grayek S, Staneva J (2021) Impacts of the Assimilation of Satellite Sea Surface Temperature Data on Volume and Heat Budget Estimates for the North Sea. *J Geophys Res Oceans* 126:e2020JC017059. <https://doi.org/10.1029/2020JC017059>
- Christensen KH, Sperrevik AK, Brostr om G (2018). On the Variability in the Onset of the Norwegian Coastal Current. <https://doi.org/10.1175/JPO-D-17-01117.1>
- Church JA, Clark PU, Cazenave A, Gregory JM, Jevrejeva S, Levermann A et al (2013) Sea-Level Rise by 2100. *Science* 342:1445–1445. <https://doi.org/10.1126/science.342.6165.1445-a>
- CMEMS (2022). GLOBAL OCEAN GRIDDED L4 SEA SURFACE HEIGHTS AND DERIVED VARIABLES REPROCESSED (1993-ONGOING). <https://doi.org/10.48670/MOI-00148>
- Craig A, Valcke S, Coquart L (2017) Development and performance of a new version of the OASIS coupler, OASIS3-MCT_3.0. *Geosci Model Dev* 10:3297–3308. <https://doi.org/10.5194/gmd-10-3297-2017>
- Craig PD, Banner ML (1994) Modeling Wave-Enhanced Turbulence in the Ocean Surface Layer. Available at: https://journals.ametsoc.org/view/journals/phoc/24/12/1520-0485_1994_024_2546_mwetit_2_0_co_2.xml (Accessed July 19, 2024)
- Dangendorf S, Hay C, Calafat FM, Marcos M, Piecuch CG, Berk K et al (2019) Persistent acceleration in global sea-level rise since the 1960s. *Nat Clim Change* 9:705–710. <https://doi.org/10.1038/s41558-019-0531-8>
- Davies AM, Kwong SCM, Flather RA (2000) On determining the role of wind wave turbulence and grid resolution upon computed storm driven currents. *Cont Shelf Res* 20:1825–1888. [https://doi.org/10.1016/S0278-4343\(00\)00052-2](https://doi.org/10.1016/S0278-4343(00)00052-2)
- de Boyer Mont egut C, Madec G, Fischer AS, Lazar A, Iudicone D (2004) Mixed layer depth over the global ocean: An examination of profile data and a profile-based climatology. *J Geophys Res Oceans* 109. <https://doi.org/10.1029/2004JC002378>
- Dodet G, Melet A, Ardhuin F, Bertin X, Idier D, Almar R (2019) The contribution of wind-generated waves to coastal sea-level changes. *Surv Geophys* 40:1563–1601. <https://doi.org/10.1007/s10712-019-09557-5>
- ECMWF (2019). IFS Documentation CY46R1 - Part VII: ECMWF Wave Model. <https://doi.org/10.21957/21G1HOIUO>
- Fan Y, Hwang P (2017) Kinetic energy flux budget across air-sea interface. *Ocean Model* 120:27–40. <https://doi.org/10.1016/j.ocemod.2017.10.010>
- Fox-Kemper B, Hewitt HT, Xiao C, A algeirsd ottir G, Drijfhout SS, Edwards TL, Golledge NR, Hemer M, Kopp RE, Krinner G, Mix A, Notz D, Nowicki S, Nurhati IS, Ruiz L, Sall e J-B, Slangen ABA, Yu Y (2023) Ocean, Cryosphere, and Sea Level Change, in *Climate Change 2021 – The Physical Science Basis: Working Group I Contribution to the Sixth Assessment Report of the Intergovernmental Panel on Climate Change*, ed. Masson-Delmotte V, Zhai P, Pirani A, Connors SL, P ean C, Berger S, Caud N, Chen Y, Goldfarb L, Gomis MI, Huang M, Leitzell K, Lonnoy E, Matthews JBR, Maycock TK, Waterfield T, Yelek ci O, Yu R, Zhou B (Cambridge University Press). <https://doi.org/10.1017/9781009157896>
- Frederikse T, Landerer F, Caron L, Adhikari S, Parkes D, Humphrey VW et al (2020) The causes of sea-level rise since 1900. *Nature* 584:393–397. <https://doi.org/10.1038/s41586-020-2591-3>
- Gasparin F, Greiner E, Lellouche J-M, Legalloudec O, Garric G, Drillet Y et al (2018) A large-scale view of oceanic variability from 2007 to 2015 in the global high resolution monitoring and forecasting system at Mercator O cean. *J Mar Syst* 187:260–276. <https://doi.org/10.1016/j.jmarsys.2018.06.015>
- Gerbi GP, Trowbridge JH, Terray EA, Plueddemann AJ, Kukulka T (2009). Observations of Turbulence in the Ocean Surface Boundary Layer: Energetics and Transport. <https://doi.org/10.1175/2008JPO4044.1>
- Geruo A, Wahr J, Zhong S (2013) Computations of the viscoelastic response of a 3-D compressible Earth to surface loading: an application to Glacial Isostatic Adjustment in Antarctica and Canada. *Geophys J Int* 192:557–572. <https://doi.org/10.1093/gji/ggs030>
- G unther H, Hasselmann S, Janssen P (1992) The wam model cycle 4.0. User manual. Deutsches klimarechenzentrum Hamburg. Tech. rep
- Hasselmann K (1970) Wave-driven inertial oscillations. *Geophys Fluid Dyn* 1:463–502. <https://doi.org/10.1080/03091927009365783>
- Hemer MA, Fan Y, Mori N, Semedo A, Wang XL (2013) Projected changes in wave climate from a multi-model ensemble. *Nat Clim Change* 3:471–476. <https://doi.org/10.1038/nclimate1791>
- Hersbach H, Bell B, Berrisford P, Hirahara S, Hor anyi A, M unoz-Sabater J et al (2020) The ERA5 global reanalysis. *Q J R Meteorol Soc* 146:1999–2049. <https://doi.org/10.1002/qj.3803>
- Hordoir R, Axell L, L optien U, Dietze H, Kuznetsov I (2015) Influence of sea level rise on the dynamics of salt inflows in the Baltic Sea. *J Geophys Res Oceans* 120:6653–6668. <https://doi.org/10.1002/2014JC010642>
- Hu A, Bates SC (2018) Internal climate variability and projected future regional steric and dynamic sea level rise. *Nat Commun* 9:1068. <https://doi.org/10.1038/s41467-018-03474-8>
- Hu H, Wang J (2010) Modeling effects of tidal and wave mixing on circulation and thermohaline structures in the Bering Sea: Process

- studies. *J Geophys Res Oceans* 115. <https://doi.org/10.1029/2008JC005175>
- Hughes CW, Fukumori I, Griffies SM, Huthnance JM, Minobe S, Spence P et al (2019) Sea level and the role of coastal trapped waves in mediating the influence of the open ocean on the coast. *Surv Geophys* 40:1467–1492. <https://doi.org/10.1007/s10712-019-09535-x>
- Hurrell JW, Deser C (2009) North Atlantic climate variability: The role of the North Atlantic Oscillation. *J Mar Syst* 78:28–41. <https://doi.org/10.1016/j.jmarsys.2008>
- Janssen PAEM (1989) Wave-Induced Stress and the Drag of Air Flow over Sea Waves. Available at: https://journals.ametsoc.org/view/journals/phoc/19/6/1520-0485_1989_019_0745_wisatd_2_0_co_2.xml (Accessed July 19, 2024)
- Janssen P (2004) The interaction of ocean waves and wind. Cambridge University Press, Cambridge. <https://doi.org/10.1017/CBO9780511525018>
- Jones JE, Davies AM (1998) Storm surge computations for the Irish Sea using a three-dimensional numerical model including wave–current interaction. *Cont Shelf Res* 18:201–251. [https://doi.org/10.1016/S0278-4343\(97\)00062-9](https://doi.org/10.1016/S0278-4343(97)00062-9)
- Komen GJ, Cavaleri L, Donela M, Hassellmann K, Janssen P (1994) Dynamics and modelling of ocean waves. *J Fluid Mech* 307:375–376. <https://doi.org/10.1017/S0022112096220166>
- Lellouche J-M, Greiner E, Le Galloudec O, Garric G, Regnier C, Drevillon M et al (2018) Recent updates to the Copernicus Marine Service global ocean monitoring and forecasting real-time 1/12° high-resolution system. *Ocean Sci* 14:1093–1126. <https://doi.org/10.5194/os-14-1093-2018>
- Levitus S, Antonov JI, Boyer TP, Locarnini RA, Garcia HE, Mishonov AV (2009) Global ocean heat content 1955–2008 in light of recently revealed instrumentation problems. *Geophys Res Lett* 36. <https://doi.org/10.1029/2008GL037155>
- Lewis HW, Castillo Sanchez JM, Siddorn J, King RR, Tonani M, Saulter A et al (2019) Can wave coupling improve operational regional ocean forecasts for the north-west European Shelf? *Ocean Sci* 15:669–690. <https://doi.org/10.5194/os-15-669-2019>
- Loomis BD, Luthcke SB, Sabaka TJ (2019) Regularization and error characterization of GRACE mascons. *J Geod* 93:1381–1398. <https://doi.org/10.1007/s00190-019-01252-y>
- Lyman JM, Johnson GC (2014) Estimating Global Ocean Heat Content Changes in the Upper 1800 m since 1950 and the Influence of Climatology Choice. *J Clim* 27(5):1945–57. <https://doi.org/10.1175/JCLI-D-12-00752.1>
- Madec G, Bourdallé-Badie R, Chanut J, Clementi E, Coward A, Ethé C et al (2019). NEMO Ocean Engine. <https://doi.org/10.5281/ZENODO.3878122>
- Madonna E, Li C, Grams CM, Woollings T (2017) The link between eddy-driven jet variability and weather regimes in the North Atlantic-European sector. *Q J R Meteorol Soc* 143:2960–2972. <https://doi.org/10.1002/qj.3155>
- Mangini F, Chafik L, Madonna E, Li C, Bertino L, Nilsen JEØ (2021) The relationship between the eddy-driven jet stream and northern European sea level variability. *Tellus Dyn. Meteorol. Oceanogr.* 73. Available at: <https://a.tellusjournals.se/articles/https://doi.org/10.1080/16000870.2021.1886419> (Accessed July 18, 2024)
- Meehl GA, Stocker TF, Collins WD, Friedlingstein P, Gaye AT, Gregory JM, Kitoh A, Knutti R, Murphy JM, Noda A, Raper SCB, Watterson IG, Weaver AJ, Zhao Z-C (2007) Global Climate Projections. In: Solomon S, Qin D, Manning M, Chen Z, Marquis M, Averyt KB, Tignor M, Miller HL (eds.) *Climate Change 2007: The Physical Science Basis*. Contribution of Working Group I to the Fourth Assessment Report of the Intergovernmental Panel on Climate Change. Cambridge University Press, Cambridge, United Kingdom and New York, NY, USA
- Melet A, Meyssignac B, Almar R, Le Cozannet G (2018) Underestimated wave contribution to coastal sea-level rise. *Nat Clim Change* 8:234–239. <https://doi.org/10.1038/s41558-018-0088-y>
- Mellor GL, Ezer T (1995) Sea level variations induced by heating and cooling: An evaluation of the Boussinesq approximation in ocean models. *J Geophys Res Oceans* 100:20565–20577. <https://doi.org/10.1029/95JC02442>
- Meyssignac B, Boyer T, Zhao Z, Hakuba MZ, Landerer FW, Stammer D et al (2019) Measuring Global Ocean Heat Content to Estimate the Earth Energy Imbalance. *Front Mar Sci* 6:432. <https://doi.org/10.3389/fmars.2019.00432>
- O’Dea EJ, Arnold AK, Edwards KP, Furner R, Hyder P, Martin MJ et al (2012) An operational ocean forecast system incorporating NEMO and SST data assimilation for the tidally driven European North-West shelf. *J Oper Oceanogr* 5:3–17. <https://doi.org/10.1080/1755876X.2012.11020128>
- Oppenheimer M, Glavovic B, Hinkel J, Van de Wal R, Magnan AK, Abd-Elgawad A et al (2019) Sea level rise and implications for low lying islands, coasts and communities. Available at: <http://repositorio.catie.ac.cr/handle/11554/9280>. Accessed Dec 27 2023
- Palmer MD, Roberts CD, Balmaseda M, Chang Y-S, Chepurin G, Ferry N et al (2017) Ocean heat content variability and change in an ensemble of ocean reanalyses. *Clim Dyn* 49:909–930. <https://doi.org/10.1007/s00382-015-2801-0>
- Pemberton P, Löptien U, Hordoir R, Höglund A, Schimanke S, Axell L et al (2017) Sea-ice evaluation of NEMO-Nordic 1.0: a NEMO-LIM3.6-based ocean–sea-ice model setup for the North Sea and Baltic Sea. *Geosci Model Dev* 10:3105–3123. <https://doi.org/10.5194/gmd-10-3105-2017>
- Pitcher GC, Figueiras FG, Hickey BM, Moita MT (2010) The physical oceanography of upwelling systems and the development of harmful algal blooms. *Prog Oceanogr* 85:5–32. <https://doi.org/10.1016/j.pocean.2010.02.002>
- Schloen J, Stanev EV, Grashorn S (2017) Wave-current interactions in the southern North Sea: The impact on salinity. *Ocean Model* 111:19–37. <https://doi.org/10.1016/j.ocemod.2017.01.003>
- Stammer D, Cazenave A, Ponte RM, Tamisiea ME (2013) Causes for Contemporary Regional Sea Level Changes. *Annu Rev Mar Sci* 5:21–46. <https://doi.org/10.1146/annurev-marine-121211-172406>
- Stanev EV, Jacob B, Pein J (2019) German Bight estuaries: An inter-comparison on the basis of numerical modeling. *Cont Shelf Res* 174:48–65. <https://doi.org/10.1016/j.csr.2019.01.001>
- Staneva J, Alari V, Breivik Ø, Bidlot J-R, Mogensén K (2017) Effects of wave-induced forcing on a circulation model of the North Sea. *Ocean Dyn* 67:81–101. <https://doi.org/10.1007/s10236-016-1009-0>
- Staneva J, Schrum C, Behrens A, Grayek S, Ho-Hagemann H, Alari V, Breivik Ø, Bidlot J (2018) A North Sea-Baltic Sea regional coupled models: atmosphere, wind waves and ocean. In: *Proceedings of the 8th EuroGOOS International Conference*
- Sterl A, Bintanja R, Brodeau L, Gleeson E, Koenigk T, Schmith T et al (2012) A look at the ocean in the EC-Earth climate model. *Clim Dyn* 39:2631–2657. <https://doi.org/10.1007/s00382-011-1239-2>
- Stokes G (1847) On the theory of oscillatory waves. *Trans Cam Soc* 8:441–455. *Mathematical and Physical papers*
- Storto A, Bonaduce A, Feng X, Yang C (2019) Steric Sea Level Changes from Ocean Reanalyses at Global and Regional Scales. *Water* 11:1987. <https://doi.org/10.3390/w11101987>
- Storto A, Masina S, Balmaseda M, Guinehut S, Xue Y, Szekely T et al (2017) Steric sea level variability (1993–2010) in an ensemble of ocean reanalyses and objective analyses. *Clim Dyn* 49:709–729. <https://doi.org/10.1007/s00382-015-2554-9>
- Sušelj K, Sood A, Heinemann D (2010) North Sea near-surface wind climate and its relation to the large-scale circulation patterns. *Theor Appl Climatol* 99:403–419. <https://doi.org/10.1007/s00704-009-0149-2>

- Tinker J, Palmer MD, Copsey D, Howard T, Lowe JA, Hermans THJ (2020) Dynamical downscaling of unforced interannual sea-level variability in the North-West European shelf seas. *Clim Dyn* 55:2207–2236. <https://doi.org/10.1007/s00382-020-05378-0>
- Valcke S (2013) The OASIS3 coupler: a European climate modelling community software. *Geosci Model Dev* 6:373–388. <https://doi.org/10.5194/gmd-6-373-2013>
- Varlas G, Katsafados P, Papadopoulos A, Korres G (2018) Implementation of a two-way coupled atmosphere-ocean wave modeling system for assessing air-sea interaction over the Mediterranean Sea. *Atmospheric Res* 208:201–217. <https://doi.org/10.1016/j.atmosres.2017.08.019>
- Wahl T, Brown S, Haigh ID, Nilsen JEØ (2018) Coastal Sea Levels, Impacts, and Adaptation. *J Mar Sci Eng* 6:19. <https://doi.org/10.3390/jmse6010019>
- Wahle K, Staneva J, Koch W, Fenoglio-Marc L, Ho-Hagemann HTM, Stanev EV (2017) An atmosphere–wave regional coupled model: improving predictions of wave heights and surface winds in the southern North Sea. *Ocean Sci* 13:289–301. <https://doi.org/10.5194/os-13-289-2017>
- WAMDI-Group TW (1988) The WAM model—a third generation ocean wave prediction model. Available at: https://journals.ametsoc.org/view/journals/phoc/18/12/1520-0485_1988_018_1775_twmngo_2_0_co_2.xml. Accessed 2 Aug 2024
- Winther NG, Johannessen JA (2006) North Sea circulation: Atlantic inflow and its destination. *J. Geophys. Res. Oceans* 111. <https://doi.org/10.1029/2005JC003310>
- Wu L, Staneva J, Breivik Ø, Rutgersson A, Nurser AJG, Clementi E et al (2019) Wave effects on coastal upwelling and water level. *Ocean Model* 140:101405. <https://doi.org/10.1016/j.ocemod.2019.101405>